# Polariton localization and dispersion properties of disordered quantum emitters in multi-mode microcavities: Supplementary Information

Georg Engelhardt<sup>1,2,3</sup> and Jianshu Cao<sup>4\*</sup>

<sup>1</sup>Shenzhen Institute for Quantum Science and Engineering,
Southern University of Science and Technology, Shenzhen 518055, China

<sup>2</sup>International Quantum Academy, Shenzhen 518048, China

<sup>3</sup> Guangdong Provincial Key Laboratory of Quantum Science and Engineering,
Southern University of Science and Technology, Shenzhen, 518055, China.

<sup>4</sup>Department of Chemistry, Massachusetts Institute of Technology,
77 Massachusetts Avenue, Cambridge, Massachusetts 02139, USA

(Dated: April 5, 2023)

## I. ANALYTICAL CALCULATIONS

## A. System

We model an ensemble of disordered quantum emitters in a microcavity by the multi-mode disordered Tavis-Cummings Hamiltonian

$$\hat{H} = \hat{H}_{\mathrm{M}} + \hat{H}_{\mathrm{L}} + \hat{H}_{\mathrm{LM}},\tag{1}$$

where

$$\hat{H}_{\rm M} = \sum_{j=1}^{N} E_j \hat{B}_j^{\dagger} \hat{B}_j, \qquad \hat{H}_{\rm L} = \sum_{k} \omega_k \hat{a}_k^{\dagger} \hat{a}_k,$$

$$\hat{H}_{\rm LM} = \sum_{j=1}^{N} \sum_{k} g_{j,k} \hat{B}_j^{\dagger} \hat{a}_k + \text{H.c.} \qquad (2)$$

Here, j and k label the quantum emitters  $\hat{B}_j$  and the photonic modes  $\hat{a}_k$ , respectively, both fulfilling a bosonic commutation relation. The quantum emitters can represent atoms, molecules or particle-hole pairs. For concreteness, we specify to molecules in this work. The excitation energies of the molecules  $E_j$  are distributed according to a probability distribution P(E). In this work, we mainly consider a Gaussian distribution,

$$P(E) = \frac{1}{\sqrt{\pi}\sigma} e^{-\frac{(E - E_{\rm M})^2}{2\sigma^2}}$$
 (3)

with center  $E_{\rm M}$  and width  $\sigma$ , but our findings are also valid for arbitrary disorder models. We consider a onedimensional translational-invariant system of length L with a periodic boundary condition. The molecules are located at positions  $r_j = j/N \cdot L$ . The photonic dispersion relation is given by

$$\omega_k = \sqrt{c^2 q_k^2 + E_C^2},\tag{4}$$

with  $q_k = 2\pi k/L$  and integer k. The confinement energy  $E_{\rm C}$  appears because of the spatial confinement of

the light field in the transversal direction of the microcavity. The photonic mode functions are given by  $\varphi_k(r) = e^{iq_k r}/\sqrt{L}$ . The light-matter coupling is parameterized by  $g_{j,k} = g_k \varphi_k(r_j)$ . As the excitation number  $\sum_k \hat{a}_k^{\dagger} \hat{a}_k + \sum_j \hat{B}_j^{\dagger} \hat{B}_j$  is an integral of motion, we focus on the single-excitation manifold for simplicity. In this work, we derive a closed-form expression for the Green's function of the multi-mode Tavis-Cummings model in the thermodynamic limit, that we define by  $N, L \to \infty$  for a constant molecule density  $\rho = N/L$ .

#### B. No disorder

Without disorder  $\sigma=0$ , all molecule energies are equal  $E_j=E_{\rm M}$  and the Hamiltonian can be easily diagonalized. Transforming the molecule operators into wavevector space,  $\hat{B}_k=\frac{1}{\sqrt{N}}\sum_{j=1}^N e^{iq_kr_j}\hat{B}_j$ , we find that the Hamiltonian is block diagonal in k and reads as

$$\hat{H} = \sum_{k} \hat{H}_{k},$$

$$\hat{H}_{k} = E_{\mathcal{M}} \hat{B}_{k}^{\dagger} \hat{B}_{k} + \omega_{k} \hat{a}_{k}^{\dagger} \hat{a}_{k} + g \sqrt{\rho} \left[ \hat{B}_{k}^{\dagger} \hat{a}_{k} + \text{h.c.} \right], \quad (5)$$

where we have assumed a constant  $g_k$  for simplicity. For each k, the two energies correspond to the lower and upper polaritons and are given as

$$E_{k,lo/up} = \frac{\omega_k + E_{\rm M}}{2} \mp \frac{1}{2} \sqrt{(\omega_k - E_{\rm M})^2 + \Omega^2},$$
 (6)

where we have defined the Rabi splitting of the disorderfree system  $\Omega=2g\sqrt{\rho}$ . The dispersion relations of the lower and upper polariton branches are depicted in Figs. 1 - 3 by dashed lines. The corresponding eigenstates are

$$|\Psi_{lo}(k)\rangle = \left[\cos(\theta)\hat{a}_k^{\dagger} + \sin(\theta)\hat{B}_k^{\dagger}\right]|\text{vac}\rangle,$$
  
$$|\Psi_{up}(k)\rangle = \left[-\sin(\theta)\hat{a}_k^{\dagger} + \cos(\theta)\hat{B}_k^{\dagger}\right]|\text{vac}\rangle, \qquad (7)$$

where

$$\theta = \frac{1}{2} \arctan \left[ \frac{g_k \sqrt{\rho}}{(\omega_k - E_{\rm M})} \right] + \frac{\pi}{2} \theta \left( \omega_k - E_{\rm M} \right)$$
 (8)

<sup>\*</sup> jianshu@mit.edu

with the Heaviside function  $\Theta(x)$ .

Crucially, all molecule operators  $\hat{B}_k$  are coupled to the photonic operators  $\hat{a}_k$  with the same wavevector. Thus, in contrast to single-mode models, there are no dark states in the system. However, for very large k, the photonic energy  $\omega_k$  by far exceeds the molecule excitation energy  $E_{\rm M}$  such that  $E_{k,lo} \to E_{\rm M}$  and  $\theta \to \pi/2$ . In this limit, the photon modes and molecule modes k are nearly decoupled such that the molecule mode k can be considered as dark. We follow the approach suggested in Ref. [1] and classify an eigenstate according to its photon weight as dark or bright. Without disorder, the photon and molecule weights of the lower polariton are defined by

$$W^{(L)}(E_{k,lo}) = \sin^2(\theta),$$
  
 $W^{(M)}(E_{k,lo}) = \cos^2(\theta).$  (9)

Accordingly, one can define the weights for the upper polariton. As suggested by Ref. [1], an eigenstate is classified as dark, when its photon weight is below a threshold value. In this work, we adopt the threshold value  $W_{th}^{(\rm L)}(E)=10\%$ . For disordered systems, a general definition of the photon and molecule weights is given in Eq. (30).

#### C. Heisenberg equations of motion

The analytical solution for the system operators  $\hat{B}_j$  and  $\hat{a}_k$  can be obtained in Laplace space. This solution can then be used to construct arbitrary Green's functions. The Heisenberg equations for the operators in the multi-mode Tavis-Cummings model read as

$$\partial_t \hat{B}_j = -iE_j \hat{B}_j - i \sum_k g_{j,k} \hat{a}_k,$$

$$\partial_t \hat{a}_k = -i\omega_k \hat{a}_k - i \sum_k g_{j,k} \hat{B}_j.$$
(10)

Transforming into the Laplace space defined by  $\hat{f}(z) = \int_0^\infty dt e^{-zt} \hat{f}(t)$  for arbitrary operators  $\hat{f}(t)$ , the equations of motions become

$$z\hat{B}_{j} - \hat{B}_{j}^{(0)} = -iE_{j}\hat{B}_{j} - i\sum_{k} g_{j,k}\hat{a}_{k},$$

$$z\hat{a}_{k} - \hat{a}_{k}^{(0)} = -i\omega_{k}\hat{a}_{k} - i\sum_{j=1}^{N} g_{j,k}^{*}\hat{B}_{j},$$
(11)

where  $\hat{B}_{j}^{(0)} = \hat{B}_{j}(0)$  and  $\hat{a}_{k}^{(0)} = \hat{a}_{k}(0)$  denote the initial conditions of the operators at time t = 0. In general, this set of coupled linear equations can not be solved analytically for a large number of photonic modes. However, we can find an exact solution in the thermodynamic limit.

To see this, we first resolve Eq. (11) and obtain

$$\hat{B}_j = \frac{\hat{B}_j^{(0)}}{z + iE_j} - i\sum_k \frac{g_{j,k}\hat{a}_k}{(z + iE_j)}.$$
 (12)

Inserting this into Eq. (11) and resolving for  $\hat{a}_k$ , we find

$$\hat{a}_{k} = \frac{\hat{a}_{k}^{(0)}}{z + i\omega_{k}(z)} - i\sum_{j=1}^{N} \frac{g_{j,k}^{*} \hat{B}_{j}^{(0)}}{(z + i\omega_{k}(z))(z + iE_{j})} - \sum_{k_{1} \neq k} \sum_{j=1}^{N} \frac{g_{j,k}^{*} g_{j,k_{1}} \hat{a}_{k_{1}}}{(z + i\omega_{k}(z))(z + iE_{j})},$$
(13)

where we have defined

$$\omega_k(z) = \omega_k - i \sum_{j=1}^N \frac{|g_{j,k}|^2}{z + iE_j}$$
$$= \omega_k - i\Pi(z). \tag{14}$$

where  $\Pi(z)$  will be denoted as self-energy. The third term in Eq. (13) represents an all-to-all coupling of the photonic modes, which cannot be solved in general. Fortunately, this term vanishes in the thermodynamic limit  $N \to \infty$ , as we explain in the following. To this end, we consider the factors

$$A_{k,k_1} = \sum_{j=1}^{N} \frac{g_{j,k}^* g_{j,k_1}}{z + iE_j}$$

$$= \sum_{j=1}^{N} \frac{g_k^* g_{k_1}}{z + iE_j} \varphi_k^*(r_j) \varphi_{k_1}(r_j)$$

$$= \frac{g^2}{L} \sum_{j=1}^{N} x_j + iy_j.$$
(15)

In the second equality, we have inserted the parameterization  $g_{j,\kappa} = g_k \varphi_k(r_j)$ . In the third line, we have introduced g as a typical measure for  $g_k$ . To explain the scaling of  $A_{k,k_1}$ , we have excluded the cavity length L normalizing the photonic mode functions  $\varphi_k(r) \propto 1/\sqrt{L}$ .

Because of the energetic disorder, the real and imaginary parts  $x_j$  and  $y_j$  are samples of random variables  $X_j$  and  $Y_j$ , respectively. According to the Gaussian law of large numbers, the means and the variances of the accumulated random variables scale as

$$\left\langle \sum_{j=1}^{N} X_{j} \right\rangle \propto \left\langle \sum_{j=1}^{N} Y_{j} \right\rangle \propto \delta_{k_{1},k},$$

$$\operatorname{Var} \sum_{j=1}^{N} X_{j} \propto \operatorname{Var} \sum_{j=1}^{N} Y_{j} \propto N.$$
(16)

Thus, the expectation values vanish except for  $k_1 = k$ , while the variances scale linearly with N. Consequently, for  $k_1 \neq k$  we find  $A_{k,k_1} \propto g^2 \sqrt{N}/L = g^2 \rho/\sqrt{N}$ . Thus, when approaching the thermodynamic limit  $N, L \to \infty$ 

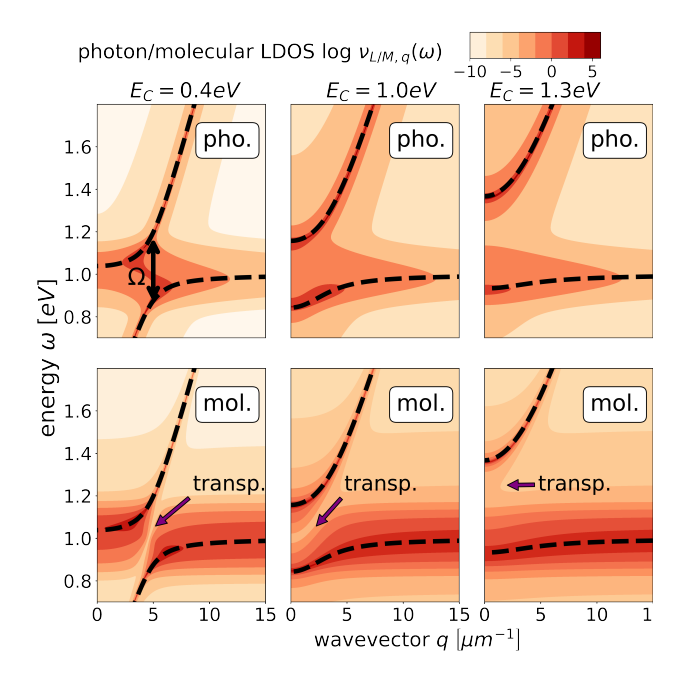


FIG. 1. Wavevector-resolved photon and molecule LDOSs for  $E_{\rm C}=0.4\,{\rm eV},~E_{\rm C}=1.0\,{\rm eV}$  and  $E_{\rm C}=1.3\,{\rm eV}.$  Overall parameters are  $L=124\,\mu{\rm m},~N=5000,~E_{\rm M}=1.0\,{\rm eV},~\sigma=0.05\,{\rm eV},$  and  $g\sqrt{\rho}=0.14\,{\rm eV}.$ 

while keeping the density  $\rho$  constant, the terms  $A_{k,k_1} \to 0$  with  $k \neq k_1$  vanish.

Combining Eq. (12) with Eq. (13), in which we neglect the third term, we obtain the following solution for the photonic modes and molecule excitations

$$\hat{a}_{k}(z) = \frac{\hat{a}_{k}^{(0)}}{z + i\omega_{k}(z)} - i\sum_{j} \frac{g_{j,k}\hat{B}_{j}^{(0)}}{(z + i\omega_{k}(z))(z + iE_{j})},$$

$$\hat{B}_{j}(z) = \frac{\hat{B}_{j}^{(0)}}{z + iE_{j}} - i\sum_{k} \frac{g_{j,k}\hat{a}_{k}^{(0)}}{(z + iE_{j})(z + i\omega_{k}(z))}$$

$$-\sum_{k} \sum_{j,l} \frac{g_{j,k}g_{j,l}^{*}\hat{B}_{j,l}^{(0)}}{(z + iE_{j})(z + i\omega_{k}(z))(z + iE_{j,l})}, (17)$$

respectively.

#### D. Green's function

Based on Eq. (17), one can directly obtain the retarded Green's function defined by

$$G_{k,k'}^{(L)}(z) \equiv -i \left\langle \left[ \hat{a}_k(z), \hat{a}_{k'}^{(0)\dagger} \right] \right\rangle,$$

$$G_{j,j'}^{(M)}(z) \equiv -i \left\langle \left[ \hat{B}_j(z), \hat{B}_{j'}^{(0)\dagger} \right] \right\rangle, \tag{18}$$

for photonic operators and molecule operators, respectively. As we consider bosonic operators in a non-interacting system, the expectation value in Eq. (18) does

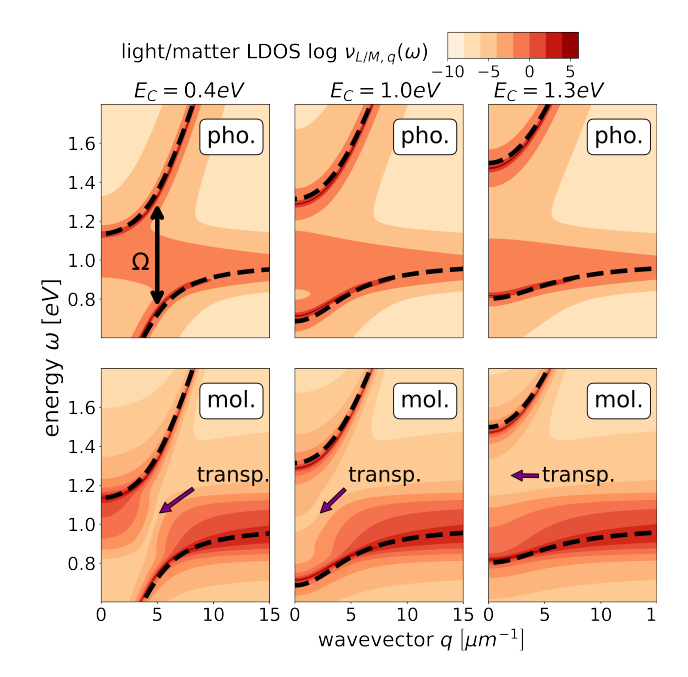


FIG. 2. Wavevector-resolved photon and molecule LDOSs for  $E_{\rm C}=0.4\,{\rm eV},~E_{\rm C}=1.0\,{\rm eV}$  and  $E_{\rm C}=1.3\,{\rm eV}.$  Overall parameters are  $L=124\,\mu{\rm m},~N=5000,~E_{\rm M}=1.0\,{\rm eV},~\sigma=0.05\,{\rm eV},$  and  $g\sqrt{\rho}=0.28\,{\rm eV}.$ 

not depend on the initial condition, which we do not specify for this reason. Explicitly, the photonic and molecule Green's functions read as

$$G_{k,k'}^{(L)}(z) = \delta_{k,k'} \frac{-i}{z + i\omega_k(z)},$$

$$G_{j,j'}^{(M)}(z) = \frac{-i}{z + iE_j} \delta_{j,j'}$$

$$+ i \sum_{k} \frac{g_{j,k} g_{j',k}^*}{(z + iE_j)(z + i\omega_k(z))(z + iE_{j'})}.(19)$$

Similarly, mixed light-matter Green's functions can be constructed. Using the photonic mode functions, we can express the photon Green's function in position space as

$$G_{j,j'}^{(L)}(z) = i \sum_{k} \frac{\varphi_k(r_j)\varphi_k^*(r_{j'})}{z + i\omega_k(z)}.$$
 (20)

# E. Disorder average

We define the disorder-averaged Green's function as

$$\overline{G}_{a,a'}^{(X)}(z) = \lim_{N \to \infty} \int \left[ \prod_{i=1}^{N} dE_i P(E_i) \right] G_{a,a'}^{(X)}(z), \quad (21)$$

where  $X \in \{L, M\}$ , and a, a' can label position j or wavevector k.

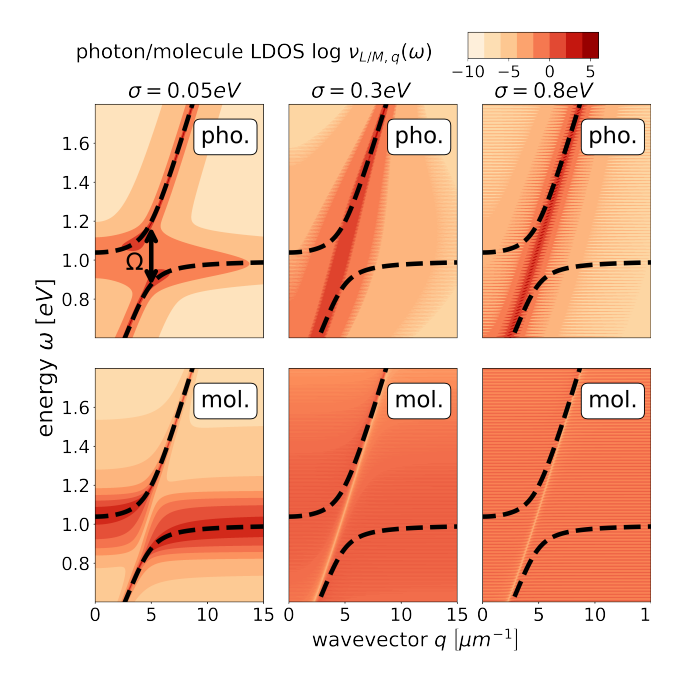


FIG. 3. Wavevector-resolved photon and molecule LDOS for three different disorders  $\sigma$  for a Gaussian disorder distribution. Overall parameters are  $E_{\rm C}=0.4\,{\rm eV},\ L=124\,\mu{\rm m},\ N=5000,\ E_{\rm M}=1.0\,{\rm eV},\ {\rm eV},\ {\rm and}\ g\sqrt{\rho}=0.14\,{\rm eV}.$ 

#### 1. Self-energy

We observe that the photonic Green's function in Eq. (19) depends on the disorder via the self energy  $\Pi(z)$  in the renormalized frequencies  $\omega_k(z)$  in Eq. (14). Using  $|g_{k,j}|^2 = g_k^2/L$ , the self-energy becomes

$$\Pi(z) = \lim_{N \to \infty} \sum_{j=1}^{N} \frac{|g_{k,j}|^2}{(z + iE_j)}$$

$$\to N \int dE P(E) \left[ \frac{1}{L} \frac{|g_k|^2}{(z + iE)} \right]$$

$$= |g_k|^2 \cdot \rho \cdot i\Gamma(z). \tag{22}$$

As the summation in the first line does not depend on the position, the sum over N can be interpreted as an integral over the energy weighted by the disorder distribution P(E) for  $N \to \infty$ . Finally, we have introduced the disorder-averaged Green's function of the uncoupled molecules

$$\Gamma(z) = -i \int dE \frac{P(E)}{(z+iE)}.$$
 (23)

The key point in this derivation is that the self-energy term is self-averaging in the thermodynamic limit and thus does not require the external averaging operations defined in Eq. (21).

## 2. Disorder-averaged Green's function

Given that the self energy is self averaging, it is now straight forward to perform the disorder average of the Green's function in Eq. (19). Apart from  $\omega_k(z)$ , the photon Green's function does not depend on the molecule energies such that the disorder-averaged Green's functions coincides with the expressions in Eqs. (19) and (20) in position and wavevector space, respectively.

The disorder average of the matter function has the effect that the terms  $1/(z+iE_j)$  are replaced by  $i\Gamma(z)$  in Eq. (23), i.e.,

$$G_{j,j'}^{(\mathrm{M})}(z) = \left[\Gamma(z)\delta_{j,j'} - i\Gamma^2(z)\sum_k |g_k|^2 \frac{\varphi_k(r_j)\varphi_k^*(r_{j'})}{z + i\omega_k(z)}\right], \quad (24)$$

which in momentum space becomes

$$G_{k,k'}^{(\mathrm{M})}(z) = \delta_{k,k'} \left[ \Gamma(z) - i\Gamma^2(z) \frac{|g_k|^2 \rho}{z + i\omega_k(z)} \right]. \tag{25}$$

We emphasize that these Green's functions are exact in the thermodynamic limit  $N \to \infty$  because of the self-averaging property of the self energy. Formally, the self average is equivalent to the celebrated coherent potential approximation (CPA). However, we emphasize that the CPA is exact for arbitrary disorder distributions for the model considered here. This is in contrast to nearest-neighbor and other short-range hopping models, where the CPA is only exact for the Lorentzian disorder model [2].

Noteworthy, the Greens function in wavevector space  $G_{k,k'}^{(\mathrm{L})}(z)$  in Eq. (19) and  $G_{k,k'}^{(\mathrm{M})}(z)$  in Eq. (25) are identical to the Green's function of the single-mode Tavis-Cummings model when replacing the photonic dispersion relation  $\omega_k$  by the energy of the single cavity mode  $\omega_C$ . The single-mode model with Lorentzian disorder has been investigated in detail in Ref. [3]. This shows that spectroscopic quantities, which can be wavevectorresolved measured, can be correctly calculated using single-mode models. In contrast, the Greens's functions in positions space given in Eq. (20) and (24) involve a summation of the wavevector. Therefore, we conclude that transport quantities and the coherence length cannot be accurately investigated in single-mode models. Thereby, the wave-vector summation in Eq. (20) and (24) ensures that the speed-of light is maintained as an upper bound in the dynamics.

## F. Photon and molecule local density of states

In terms of the eigenstates  $|\alpha\rangle$  and energies  $\epsilon_{\alpha}$  of the Hamiltonian in Eq. (1), we define the wavevector-resolved

photon and molecule local density of states (LDOS) via

$$\nu_{L,k}(\omega) = \frac{1}{2\delta} \sum_{\epsilon_{\alpha} \in [\omega - \delta, \omega + \delta]} \langle \alpha | \, \hat{a}_{k}^{\dagger} \hat{a}_{k} \, | \alpha \rangle \,,$$

$$\nu_{M,k}(\omega) = \frac{1}{2\delta} \sum_{\epsilon_{\alpha} \in [\omega - \delta, \omega + \delta]} \langle \alpha | \, \hat{B}_{k}^{\dagger} \hat{B}_{k} \, | \alpha \rangle \qquad (26)$$

with an infinitesimal  $\delta > 0$ . We note that the photon and molecule LDOS can be measured by angular-resolved spectroscopy. The diagonal elements of the Green's function in Eq. (18) can be formally written as

$$G_{k,k}^{(\mathrm{L})}(z) \equiv -i \sum_{\alpha} \frac{\Psi_{\alpha}^{(\mathrm{L})}(q_k) \Psi_{\alpha}^{(\mathrm{L})*}(q_k)}{z + i\epsilon_{\alpha}},$$

$$G_{k,k}^{(\mathrm{M})}(z) \equiv -i \sum_{\alpha} \frac{\Psi_{\alpha}^{(\mathrm{M})}(q_k) \Psi_{\alpha}^{(\mathrm{M})*}(q_k)}{z + i\epsilon_{\alpha}},$$
(27)

where  $\Psi_{\alpha}^{(\mathrm{L})}(q_k) = \langle \alpha | \hat{a}_k^{\dagger} | \mathrm{vac} \rangle$  and  $\Psi_{\alpha}^{(\mathrm{M})}(q_k) = \langle \alpha | \hat{B}_k^{\dagger} | \mathrm{vac} \rangle$  are the eigenstates in wavevector representation. Using the Dirac identity  $\lim_{\delta \downarrow 0} 1/(x+i\delta) = \mathcal{P}1/x - i\pi\delta(x)$ , it is now straightforward to show that

$$\nu_k^{(X)}(\omega) = -\lim_{\delta \downarrow 0} \frac{1}{\pi} \operatorname{Im} G_{k,k}^{(X)}(-i\omega + \delta)$$
 (28)

for  $X \in \{L, M\}$ . For later purpose, we also define the total density of states

$$\nu(\omega) \equiv \frac{N_{\omega,\delta}}{2\delta}$$

$$= \sum_{k} \left[\nu_{L,k}(\omega) + \nu_{M,k}(\omega)\right], \qquad (29)$$

where  $N_{\omega,\delta}$  is the number eigenstates in the energy interval  $[\omega - \delta, \omega + \delta]$  having an infinitesimal width  $2\delta$ . The equality in the second line follows from the fact that  $\sum_k \left[ \hat{a}_k^{\dagger} \hat{a}_k + \hat{B}_k^{\dagger} \hat{B}_k \right] = 1$  in the single-excitation manifold.

In Fig. 1, we analyze the photon and molecule LDOSs for three confinement energies  $E_{\rm C}=0.4\,{\rm eV},\ E_{\rm C}=1.0\,{\rm eV}$  and  $E_{\rm C}=1.3\,{\rm eV}$ . For simplicity we assume a wavevector-independent light-matter interaction  $g_k=g$ . All three photon and molecule LDOSs look qualitatively similar. Yet, we find that the photon LDOS for  $E_{\rm C}=1.3\,{\rm eV}$  has a significant smaller contribution for energies close to  $E_{\rm M}$  than the ones for  $E_{\rm C}=0.4\,{\rm eV}$  and  $E_{\rm C}=1.0\,{\rm eV}$ . In contrast, the matter LDOS for  $E_{\rm C}=1.3\,{\rm eV}$  has a significant smaller contribution close to the photon dispersion  $\omega_k$  than the ones for  $E_{\rm C}=0.4\,{\rm eV}$  and  $E_{\rm C}=1.0\,{\rm eV}$ .

In Fig. 2, we analyze the LDOSs for the same parameters as in Fig. 1, but for a larger light-matter coupling. Accordingly, we see that now the Rabi splitting  $\Omega=2\sqrt{\rho}g$  is significantly larger. Consequently, the transparency effect in the matter LDOS within the gap is better visible.

Next, we investigate the influence of disorder on the

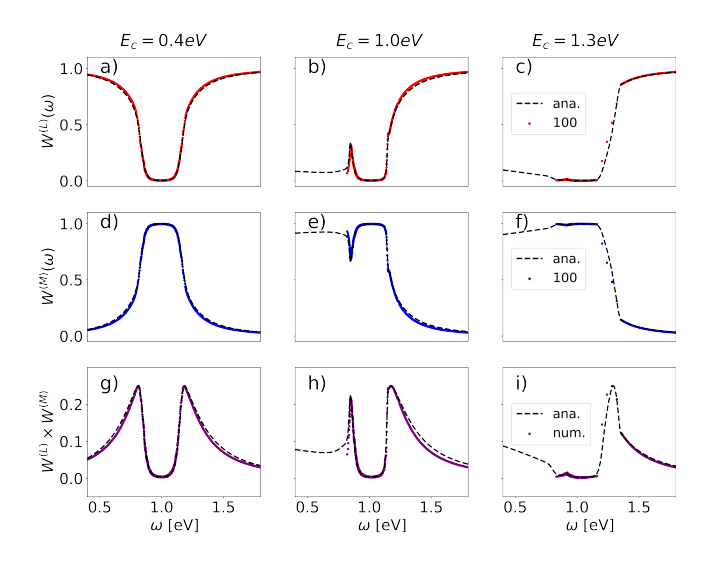


FIG. 4. Investigation of the photonic weight  $W^{(L)}(\omega)$  [panels (a), (b), and (d)] and matter weight  $W^{(M)}(\omega)$  [panels (d), (e), and (f)] defined in Eq. (31). Panels (g), (h), and (i) depict the product  $W^{(L)}(\omega) \cdot W^{(M)}(\omega)$  as a measure for the light-matter mixing. Overall parameters are the same as in Fig. 1.

photon and molecule LDOSs, which is depicted in Fig. 3 for three different  $\sigma$ . For  $\sigma = 0.05\,\mathrm{eV}$ , we observe two separate polariton bands, that merged for  $\sigma = 0.3\,\mathrm{eV}$ . When further increasing to  $\sigma = 0.8\,\mathrm{eV}$ , the photon LDOS increasingly concentrates around the photon dispersion relation  $\omega_k$ : for increasing  $\sigma$ , the molecular excitation energies are distributed over a larger energy range, which leads to an increasing decoupling of photonic and molecular systems, analog to the behavior in single-mode models [3].

# G. Photon and molecule weights

The photon and molecule weights of a polariton determine its dynamical properties. In terms of the eigenstates  $|\alpha\rangle$  of the multi-mode Tavis-Cummings Hamiltonian, these quantities are defined as

$$W^{(X)}(\epsilon_{\alpha}) \equiv \langle \alpha | \sum_{k} \hat{a}_{k}^{\dagger} \hat{a}_{k} | \alpha \rangle, \qquad (30)$$

where  $X \in \{L, M\}$ . In the numerical calculations, we evaluate the averaged quantities

$$W^{(X)}(\omega) = \frac{1}{N_{\omega,\delta}} \sum_{\epsilon_{\alpha} \in [\omega - \delta, \omega + \delta]} W^{(X)}(\epsilon_{\alpha}), \quad (31)$$

where  $N_{\omega,\delta}$  is the number of eigenstates in the energy interval  $[\omega - \delta, \omega + \delta]$  of width  $2\delta \ll \omega$ . Note that due to their definition, the photon and matter weights sum up to one, i.e.,  $W^{(L)}(\omega) + W^{(M)}(\omega) = 1$ . Using the definitions of the wavevector-resolved LDOS in Eq. (26) and the total

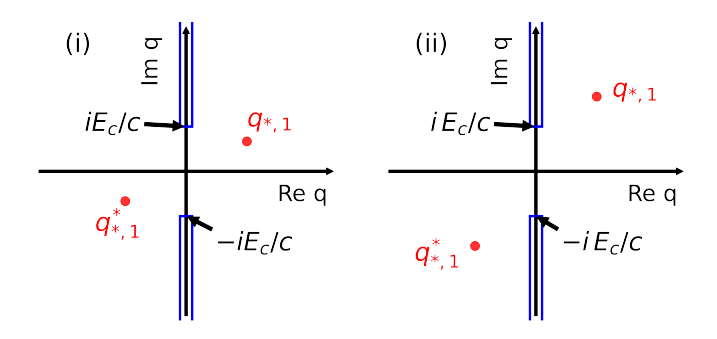


FIG. 5. Sketch of the nonanalyticities of the Green's function in the complex q plain, that determine the asymptotic behavior of the Fourier transformation in Eq. (33). The branch cut of the integrand  $G_q$  are depicted by blue contours. The poles of  $G_q$  are marked by red points.

density of states in Eq. (29), we find

$$W^{(X)}(\omega) = \sum_{k} \frac{\nu_k^{(X)}(\omega)}{\nu(\omega)}.$$
 (32)

Thus, the photon (molecule) weight is the photon (molecule) LDOS integrated over the wavevector k and normalized by the total density of states. This expression can be numerically integrated using the analytical expression of the Greens's functions in Eq. (19) and (25).

In Fig. 4 (a) - (c) we depict the photon weight as a function of energy for three different confinement energies  $E_{\rm C}$ . These plots serve also as a benchmark calculation of our analytical solution in Eqs. (19) and (25). Thereby, the weights have been numerically evaluated using Eq. (31), where the eigenstates  $|\alpha\rangle$  have been obtained by numerical diagonalization of the Hamiltonian. In panels (a)-(c) we observe a significant dip in the photon weight for energies around  $\omega \approx E_{\rm M}$ . As the photon weight is less than  $W^{(L)} < 10\%$ , these eigenstates are classified as dark states according to the explanations in Sec. IB. In panel (b) and (c) we find that the photon weight is larger than  $W^{(L)} = 50\%$  only for energies above  $E_{\rm M}$ , as the photonic dispersion relation is bounded by  $E_{\rm C}$  from below. The panels Fig. 4 (d) - (f) depict the corresponding matter weights. Moreover, we depict the light-matter mixing, which we define as the product  $W^{(L)}(\omega) \cdot W^{(M)}(\omega)$ . The peaks of this quantity clearly resembles the lower and upper polariton bands.

## H. Asymptotic behavior in position space

Next, we are interested in the asymptotic behavior of the Green's function in position space, i.e., we investigate  $G_{j,j'}^{(X)}(-i\omega^+)$  for  $X \in \{L,M\}$  and large  $|r_j - r_{j'}|$ , where  $\omega^+ = \omega + i\delta$  with infinitesimal  $\delta > 0$ . From Eqs. (19) and

(20) we see that the matter Green's function is proportional to the photon Green's function when  $g_k$  changes only slowly with k, such that we continue to investigate the latter, which reads in the continuum limit  $L \to \infty$ 

$$G_{j,j'}^{(L)}\left(-i\omega^{+}\right) = \int_{-\infty}^{\infty} G_{q}(-i\omega)e^{iq\left(r_{j}-r_{j'}\right)}dq,$$

$$G_{q}(-i\omega) = \frac{-i}{-i\omega + i\omega_{qL/2\pi} + ig_{qL/2\pi}^{2}\rho\Gamma(-i\omega)},$$
(33)

On the right hand side we can replace  $\omega^+ \to \omega$  as the poles of the Green's function are not located on the real axes because of the complex-valued  $\Gamma(z)$ .

We can analyze the asymptotic behavior of the Green's function using a theorem of functional analysis [4]:

Let f be in  $L^2(\mathbb{R}^n)$  (space of square-integrable functions). Then  $e^{b|x|}f \in L^2(\mathbb{R}^n)$  for all b < a if and only if its Fourier transformation  $\tilde{f}$  has an analytic continuation to the set  $\{\zeta \mid |\zeta| < a\}$  with the property that for each  $\eta \in \mathbb{R}^n$  with  $|\eta| < a$ ,  $\tilde{f}(\cdot + i\eta) \in L^2(\mathbb{R}^n)$  and for any b < a:  $\sup_{|\eta| < b} ||f(\cdot + i\eta)||_2 < \infty$ .

Applied to the Fourier transformation in Eq. (33), this theorem states that the asymptotic behavior of the Green's function is determined by the poles and branch cuts of the integrand (i.e., the Green's function in wavevector space), where q is now interpreted as a complex variable.

For simplicity, we consider the case  $g_k = g$ . In this case the integrand  $G_q$  is nonanalytic at

$$q_{*,1} = \frac{1}{c} \sqrt{[\omega - g^2 \rho \Gamma(-i\omega)]^2 - E_{\rm C}^2},$$

$$q_{*,2} = i \frac{E_{\rm C}}{c},$$
(34)

as well as the complex conjugate values. Thereby,  $q_{*,1}$  appears because of the pole of the Green's function  $G_q$ ,  $q_{*,2}$  appears because of the branch cut induced by the photonic dispersion relation in Eq. (4). According to the above theorem, the asymptotic behavior is mainly determined by the nonanalyticity whose imaginary part is closer to zero.

In Fig. 5, we sketch two cases: (i)  $|\text{Im }q_{*,1}| < |\text{Im }q_{*,2}|$ , and (ii)  $|\text{Im }q_{*,1}| > |\text{Im }q_{*,2}|$ . In case (i), we find that the asymptotic decay is determined by the pole of the Green's function. In this case, the coherence length depends on the light-matter interaction and other system parameters. In case (ii), the branch cut and, consequently, the ratio  $E_{\rm C}/c$  determines the asymptotic behavior. In short, the asymptotic behavior for large  $r = |r_j - r_{j'}|$  can be written as

$$\left| G_{j,j'}^{(L)} \left( -i\omega^+ \right) \right| \to a_1 e^{-\frac{r}{2\zeta_{coh,1}}} + a_2 e^{-\frac{r}{2\zeta_{coh,2}}},$$
 (35)

where we have defined the coherence lengths

$$\zeta_{coh,i} = \frac{1}{2 \text{Im } q_{*i}} \tag{36}$$

for i=1,2. In the numerical calculations we find that the asymptotic behavior is accurately determined by  $q_{*,1}$ , see Sec. II B. For this reason, we assess that the coefficients fulfill  $a_1\gg a_2$ , and we define the system's coherence length as  $\zeta_{coh}\equiv\zeta_{coh,1}$ .

In the Letter, the coherence length for different values of the confinement energy  $E_{\rm C}$  is shown in Figs. 1(g)-(i). Comparing with the photon weight, we observe a clear correlation between both quantities, that will be explained in the next section. Consequently, the coherence length is very short in the energy range close to  $\omega \approx E_{\rm M}$ , that exhibits dark states. From this observation we conclude, that dark states have an overall destructive impact on transport properties.

It is also instructive to investigate the coherence length for a small light-matter interaction. Taylor expansion of Eq. (34) up to first order in  $g^2\rho$  results in

$$\zeta_{coh}^{-1} = \frac{1}{c} \operatorname{Im} \left[ \sqrt{\omega^2 - E_C^2} - \frac{\omega}{\sqrt{\omega^2 - E_C^2}} g^2 \rho \Gamma(-i\omega) \right] + \mathcal{O} \left[ \left( g^2 \rho \right)^2 \right],$$
(37)

which exhibits a different behavior depending on the energy  $\omega$ . For  $\omega > E_{\rm C}$ , the first term in Eq. (37) is real valued and the coherence length is essentially determined by the imaginary part of  $\Gamma(-i\omega)$ . This analysis thus reveals why the coherence length decreases  $g^2\rho$  in Fig. 3(a) and (c) in the Letter for  $\omega > E_{\rm C}$ . As the imaginary part of  $\Gamma(-i\omega)$  is given by the molecular disorder distribution P(E), the coherence length is proportional to the number of molecules having excitation energy  $E_j = \omega$ . Noteworthy, for  $E_{\rm C} = 0$ , the inverse coherence length

$$\zeta_{coh}^{-1} \propto g^2 \rho P(\omega)$$
 (38)

is proportional to Beer's absorption length, which is consistent with the unraveling of the Green's function in terms of scattering processes below in Sec. II.

For  $\omega < E_{\rm C}$ , the first term becomes imaginary and gives a constant contribution to  $\zeta_{coh}^{-1}$ . Now, the real part of  $\Gamma(-i\omega)$  determines the dependence on  $g\sqrt{\rho}$ . Interestingly when the energy  $\omega$  approaches  $E_{\rm C}$  from above, the coherence length increases. Formally for  $\omega = E_{\rm C}$ , the coherence length diverges, yet, we note that the Taylor expansion is invalid in this case. Thus, from Eq. (37) we cannot conclude that the coherence length is non-analytic at  $\omega = E_{\rm C}$ .

## I. Interpretation

Interestingly, the coherence length is a function of the Rabi frequency  $\Omega = 2g\sqrt{\rho}$ . Analysis of the coherence

length shows that it scales with  $\zeta_{coh} \propto \Omega^{-2}$  for small  $\Omega$ , as can be seen in Figs. 1(a) and (c) in the Letter. In this section, we interpret this behavior in terms of photon scattering.

Expanding the photon Green's function in position space in orders of g, we obtain

$$G_{j,j'}^{(L)}(z) = \sum_{k} G_{j,j'}^{(L)}(z,k),$$

$$G_{j,j'}^{(L)}(z,k) = G_{j,j'}^{(0)}(k) + g^{2} \sum_{j_{1}=1}^{N} G_{j,j_{1}}^{(0)}(k) \Gamma_{j_{1}} G_{j_{1},j'}^{(0)}(k)$$

$$+ g^{4} \sum_{j_{1},j_{2}=1}^{N} G_{j,j_{1}}^{(0)}(k) \Gamma_{i_{1}} G_{j_{1},j_{2}}^{(0)}(k) \Gamma_{i_{2}} G_{j_{2},j'}^{(0)}(k)$$

$$+ \mathcal{O}(g^{6}), \tag{39}$$

where

$$G_{i,j}^{(0)}(k) = G_{i,j}^{(0)}(z,k) = -i\frac{\varphi_k(r_i)\varphi_k^*(r_j)}{(z+i\omega_k)},$$

$$\Gamma_j = \Gamma_j(z) = -i\frac{1}{(z+iE_j)}$$
(40)

denote the free Green's functions of the photon mode k and the molecule j, respectively. Thus, the full Green's function is a sum of k-dependent Green's functions, that can be unraveled as a series of scattering processes. The first term ( $\propto g^0$ ), describes the propagation of a photon without scattering events. The second term describes a single scattering at molecule  $j_1$ . Both absorption and emission contribute one factor g. Noteworthy, Im  $\Gamma_j(-i\omega)$  is proportional to the linear absorption of a two-level systems in dipole approximation. As there are N molecules in the cavity, this terms scales overall with  $\propto g^2N$ . Accordingly, the third term can be interpreted as two scattering events and scales with  $\propto g^4N^2$ . Each term in Eq. (39) can be interpreted as a distinct path from  $r_j$  to  $r_{j'}$ .

For increasing  $g^2N$ , more higher-order paths become relevant in the expansion in Eq. (39). Due to the random phase factors of  $\varphi_k(r_j)$ , this leads to a destructive interference between different paths, which suppresses the probability that a photon can travel from  $r_j$  to  $r_{j'}$ . This is reflected by a shorter coherence length of the Green's function.

The disorder distribution of the molecular excitation energies P(E) thereby determines the number of molecules that can take part in this scattering process. Only molecules whose excitation energy  $E_j$  exactly matches the energy of the eigenstate  $\omega(=iz)$  can resonantly scatter photons, which mediate the formation of the eigenstates. Thereby, the more a photon is scattered at molecules the smaller is the photon weight, which explains the close correspondence of photon weight and coherence length in Fig. 1 in the Letter. This analysis motivates to identify the coherence length as the absorption length known in Beer's absorption low, which opens an

alternative way for the experimental verification of the predictions in our work.

#### II. NUMERICAL CALCULATIONS

## A. Diagonalization

Before describing the details of the numerical calculations, we list here the overall parameters and procedures that are used unless stated differently. In the numerical calculations, we use an open boundary conditions instead of a periodic one, as the corresponding mode functions  $\varphi_k(r) = \sin(q_k r)/\sqrt{L/2}$  with  $q_k = \pi/L \cdot k$  are real valued. This guarantees that all eigenvalues are real, simplifying the disorder average. This is in contrast to the periodic boundary condition considered in the analytical calculations in Sec. I. Yet, away from the boundaries, the physical properties will be the same under both boundary conditions.

We consider a system with N=5000 molecules and a cavity of length  $L=124\,\mu\mathrm{m}$ . Molecule  $j\in\{1,\ldots,N\}$  is located at position  $r_j=N/L\cdot j$ . For reference, we define the resonance wavelength  $\lambda_0$  such that  $c\cdot 2\pi/\lambda_0=E_\mathrm{M}/\hbar$ . For  $E_\mathrm{M}=1\,\mathrm{eV}$ , we find that  $\lambda_0=1.24\mu\mathrm{m}$ . Thus, expressed in units of  $\lambda_0$ , the cavity length is  $L=100\lambda_0$ , and the particle density is  $\rho=N/L=50/\lambda_0$ . We quantize the photonic field with N=5000 modes, such that the cut-off energy is  $\omega_\mathrm{cut-off}=\omega_{k=5000}=\sqrt{c^2(\pi 50/L)^2+E_\mathrm{C}^2}\approx 50\cdot E_\mathrm{M}$ . In total, we average over M=50 sample Hamiltonians.

In the diagonalization, the photon and molecule subsystems are represented in the wavevector basis and position basis, respectively. The construction of the Green's function requires a transformation between these representations. We denote the elements of the photon subsystem of an eigenstates  $\alpha$  with energy  $\epsilon_{\alpha}$  by  $\Psi_{\alpha}^{(L)}(q_k)$ , and the molecule subsystem elements by  $\Psi_{\alpha}^{(M)}(r_j)$ . Using the photonic mode functions  $\varphi_k(r)$ , we can transform the photon subsystem into the position representation via

$$\Psi_{\alpha}^{(L)}(r_j) = \sqrt{\frac{L}{2N^2}} \sum_{k=1}^{N} \varphi_k(r_j) \Psi_{\alpha}^{(L)}(q_k).$$
 (41)

The additional factor  $\sqrt{L/2N}$  is required due to the discretization of the photon field in position space. It ensures that the photon weight remains unchanged in the transformation:  $W^{(L)}(\epsilon_a) = \sum_j \left|\Psi_{\alpha}^{(L)}(r_j)\right|^2 = \sum_k \left|\Psi_{\alpha}^{(L)}(q_k)\right|^2$ . Accordingly, we can transform the matter subsystem into the wavevector representation:

$$\Psi_{\alpha}^{(M)}(q_k) = \sqrt{\frac{L}{2N^2}} \sum_{j=1}^{N} \varphi_k(r_j) \Psi_{\alpha}^{(M)}(q_k).$$
 (42)

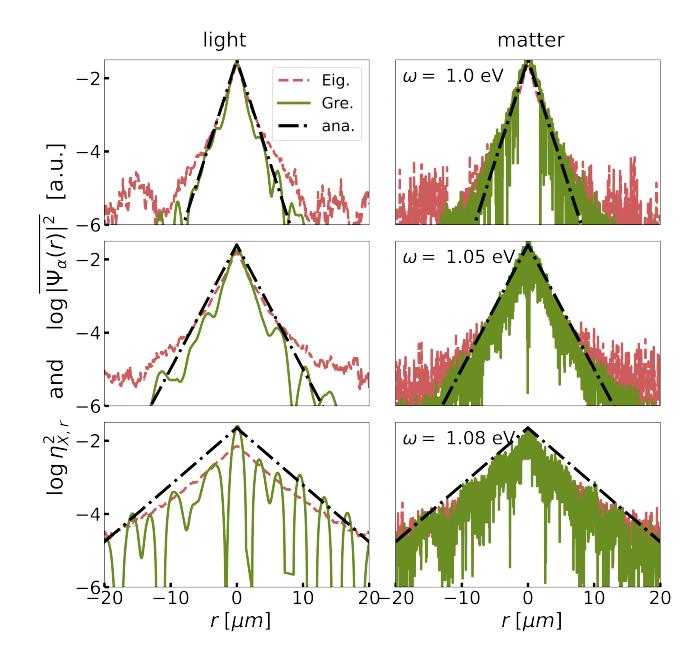


FIG. 6. Comparison of  $[\eta_{X,r}(\omega)]^2$  [defined in Eq. (46) via the imaginary part of the Green's function] and the disorder-averaged eigenstate in Eq. (47). The general diagonalization procedure is described in Sec. II A. The Green's function and eigenstates are averaged over an interval of width  $\delta = 0.01$ . The dash-dotted black lines depict the analytical predicted exponential decay with the coherence length in Eq. (36) for i = 1. Parameters are the same as in Fig. 1 and  $E_C = 0.4 \,\mathrm{eV}$ .

## B. Disorder-averaged Green's function

In terms of eigenstates, the disorder-averaged Green's function in position space can be written as

$$\overline{G}_{j,j'}^{(X)}(z) = \frac{-i}{M} \sum_{l=1}^{M} \sum_{\alpha} \frac{\Psi_{\alpha}^{(X)(l)}(r_j) \Psi_{\alpha}^{(X)(l)*}(r_{j'})}{z + i\epsilon_{\alpha}^{(l)}}, \quad (43)$$

where  $\epsilon_{\alpha}^{(l)}$  and  $\Psi_{\alpha}^{(l)}(r_j)$  are the energies and the eigenstates of the l-th sample Hamiltonian. In the following, we use that the Hamiltonian in Eq. (1) is time-reversal invariant, implying that there exist a gauge for which the eigenstates are real valued. For this reason, it is possible to express the imaginary part of the Green's function as

$$\eta_{j,j'}^{(X)}(\omega) \equiv \lim_{\delta \downarrow 0} \frac{-1}{\pi} \operatorname{Im} \overline{G}_{j,j'}^{(X)}(-i\omega + \delta) 
= \frac{1}{M} \sum_{l=1}^{M} \lim_{\delta \downarrow 0} \sum_{\epsilon_{\alpha}^{(l)} \in [\omega - \delta, \omega + \delta]} \Psi_{\alpha}^{(X)(l)}(r_{j}) \Psi_{\alpha}^{(X)(l)}(r_{j'}).$$
(44)

In the wavevector representation, the Green's function can be evaluated using

$$\overline{G}_{k,k'}^{(X)}(z) = \frac{1}{M} \sum_{l=1}^{M} \sum_{\alpha} \frac{\Psi_{\alpha}^{(X)(l)}(q_k) \Psi_{\alpha}^{(X)(l)*}(q_{k'})}{z + i\epsilon_{\alpha}^{(l)}}.$$
 (45)

As the system is translational invariant in a stochastic sense, the disorder-averaged Green's function is diagonal in the wavevector basis, i.e.,  $\overline{G}_{k,k'}^{(X)}(z) \propto \delta_{k,k'}$ .

# C. Asymptotic behavior in position space

As the disorder-averaged Green's function is translationally invariant, it can be expressed as the difference of two positions, i.e.,

$$\eta_{X,r}(\omega) \equiv \lim_{N \to \infty} \eta_{j,j'}^{(X)}(\omega),$$
(46)

where  $r = |r_j - r_{j'}|$ . Importantly, the asymptotic behavior of  $\eta_{X,r}(\omega)$  for large r exhibits the same scaling as Eq. (35).

In Fig. 6, we depict  $\eta_{X,r}^2(\omega)/\mathcal{N}$  for both  $X=\mathrm{L},\mathrm{M}$  as a function of position by a solid green line. The normalization  $\mathcal{N}$  is chosen such that the integral over the position is one. We depicted the squared function to allow for a better comparison with the disorder-averaged eigenstates defined later in Eq. (47).

The decay of the Green's function with increasing separation |r| is clearly visible for both photon and molecule Green's functions. For comparison, we have added the exponential decay predicted by the analytical coherence length  $\zeta_{coh,1}$  in Eq. (36) as a dash-dotted black line. We observe that the numerical and analytical calculations precisely agree, which is especially clearly visible for the molecule Green's function. We thus conclude that the asymptotic behavior of the Green's function is determined by  $\zeta_{coh} = \zeta_{coh,1}$  and that  $a_1 \gg a_2$  in Eq. (35). This assessment is additionally confirmed by the agreement of the analytical and numerical calculations of the coherence length shown in Fig. 1 (g)-(i) in the Letter .

In Fig. 6, the photon Green's function is more smooth than the matter contribution and exhibits a modulation as a function of separation r. The modulation frequency is determined by the real part of the root  $q_{*,1}$  in Eq. (34). We explain the deviation form a mononchromatic modulation by the finite energy integral, over which we average the Green's function in Eq. (44).

#### D. Disorder-averaged eigenstates

We define the disorder-averaged eigenstates in position space for the eigenstates  $\Psi_{\alpha}^{(X)}(r)$  within a small energy

interval  $\epsilon_{\alpha} \in [\omega - \delta, \omega + \delta]$  as

$$\overline{\left|\Psi^{(X)}(r)\right|^2} = \frac{1}{N_{\omega,\delta}} \sum_{\epsilon_{\alpha} \in [\omega - \delta, \omega + \delta]} \left|\Psi_{\alpha}^{(X)}(r - \overline{r_{\alpha}})\right|^2, \quad (47)$$

where  $x \in \{L, M\}$ ,  $N_{\omega,\delta}$  is the number of eigenstates in the energy interval, and the center of each eigenstate  $\alpha$  is given by

$$\overline{r_{\alpha}} = \frac{\sum_{j=1}^{N} r_{j} \left| \Psi_{\alpha}^{(X)}(r_{j}) \right|^{2}}{\sum_{j=1}^{N} \left| \Psi_{\alpha}^{(X)}(r_{j}) \right|^{2}}.$$
 (48)

Similarly, we can define the disorder-averaged eigenstates in wavevector space, which agrees with the Green's function in Eq. (45) for k=k'.

Guided by the analytical and numerical calculations of the Green's function, we anticipate that the exponential decay of the disorder-averaged wavefunction is dominated by one exponential term. Similar to the Green's function in Eq. (35), we thus define the coherence length  $\zeta_{loc}$  such that

$$\overline{\left|\Psi^{(X)}(r)\right|^2} \propto \exp\left[-\frac{|r|}{\zeta_{loc}(\omega)}\right]$$
 (49)

for large |r|.

In Fig. 6, we depict the disorder-averaged eigenstates and observe that the photon contribution of the wave function exponentially decays with |r|. The fluctuations are significantly less than the fluctuations in the Green's function. Interestingly, we observe that the disorder-averaged eigenstates and the Green's function exhibit the same decay behavior for small-to-intermediate |r|, i.e.,  $\zeta_{coh} \approx \zeta_{loc}$ . We attribute this agreement to the photon-mediated long-range interaction between distant molecules, which protects their coherent phase relation.

For very large |r|, the eigenstates decay significantly slower than the Green's function. These deviations can have two distinct explanations: (i) the Green's function is subject to significant destructive interference because of the average over the finite energy interval in Eq. (44). (ii) The numerical calculation suffers from a finite computational precision. Importantly, we have numerically checked that this slow decay is not determined by the branch-cut related value  $\zeta_{coh,2}$  in Eq. (36), which would predict a significantly faster decay rate.

## E. Numerical calculation of the coherence length

Because of the large fluctuations of the Green's function, extracting the coherence length via fitting is numerically unstable. Instead, we determine the coherence length via comparison with the position variance of the normalized function as follows:

We start with a generic exponentially decaying func-

tion

$$F(r) = \frac{\lambda}{2} e^{-\lambda|r|},\tag{50}$$

whose integral over  $x \in \{-\infty, \infty\}$  is one. In particular, we use  $F(r) = \eta_{\mathrm{M},r}^2(\omega)/\mathcal{N}$ . Here, we use  $X = \mathrm{M}$ , as the molecule Green's function does not exhibit (almost) monochromatic smooth modulations like the photon Green's function (c.f., Fig. 6). While for the monochromatic modulation of the photon Green's function, F(r) must be multiplied by a cosine function with an unknown frequency, the high-frequent fluctuations of the molecules Green's function simply average away. The position variance of F(r) evaluates to

$$Var_F \hat{X} = 2 \int_0^\infty \frac{\lambda}{2} r^2 e^{-\lambda r} dr$$
$$= \lambda \frac{1}{\lambda^2} \int_0^\infty e^{-\lambda x} dr$$

$$= \lambda \frac{1}{\lambda^2} \frac{1}{\lambda}$$

$$= 2\lambda \frac{1}{\lambda^3} = 2\frac{1}{\lambda^2} = 2\zeta_{coh}^2.$$
 (51)

In the last step, we have inserted the coherence length  $\zeta_{coh} = 1/\lambda$ .

This numerical approach assumes that there is only one exponentially decaying term, as opposed to the two terms predicted in Eq. (35). However, the analysis in Fig. 6 has shown that only the pole of the Green's function substantially determines the decaying behavior, while the branch-cut term can be neglected. For this reason, the deployed numerical procedure provides a value for the coherence length related to the Green's function pole. We emphasize that the precise agreement of the analytical and numerical calculations in Fig. 1(g)-(i) in the Letter justifies the numerical approach introduced here.

<sup>[1]</sup> R. F. Ribeiro, Multimode polariton effects on molecular energy transport and spectral fluctuations, Communications Chemistry 5, 48 (2022).

<sup>[2]</sup> A. Chenu and J. Cao, Construction of multichromophoric spectra from monomer data: Applications to resonant energy transfer, Phys. Rev. Lett. 118, 013001 (2017).

<sup>[3]</sup> G. Engelhardt and J. Cao, Unusual dynamical properties of disordered polaritons in microcavities, Phys. Rev. B 105, 064205 (2022).

<sup>[4]</sup> M. Reed and S. Barry, Methods of modern mathematical physics. II. Fourier analysis, self-adjointness. (Academic Press, New-York-London., 1975) section IX.3; Theorem IX.13.